Journal of Marine Research, 70, 93–117, 2012

Measuring overturns with gliders

by S. A. Thorpe[1]

ABSTRACT

The accuracy of the estimation of the vertical size of eddies in turbulent stratified shear flows in the ocean from measurements obtained by gliders is examined. It is assumed that gliders move along paths inclined at moderate angles to the horizontal. Comparison is made with measurements by probes falling or lowered vertically through billows resulting from Kelvin-Helmholtz (K-H) or Holmboe instability and through the statically unstable regions formed at early stages of convective breaking of internal waves. The probable errors involved in estimating the overturn scale of a K-H billow along the track of a glider are greatest when the ratio of the billow's vertical to horizontal scale, b/a, is greatest and when a glider's inclination angle, α, is moderate, but the errors are generally relatively small. At small angles, α, the glider path may intersect more than one billow, reducing the errors. Larger errors are possible, however, in measuring eddies in turbulent stratified shear flows, and their magnitude depends on the orientation of eddies relative to the trajectory of the glider.

False overturns may be apparent using gliders with small inclination angles, α, in internal waves, and consequently erroneous estimates of the displacement scales obtained, even when the slope of the waves, s, < 1 and convective overturn is entirely absent. Quantification of overturns from glider measurements of the apparent vertical size of the regions in which the density increases upward can result in misleading estimates of the scale of overturns. Although, because of the wave-induced horizontal and vertical motions, the trajectory of free-fall probes will not be vertical when passing through an internal wave field, and nor will it be steady, the mean square displacements obtained from measurements are found to be the same as those that would be made by a probe passing vertically through a frozen wave field. Attention is drawn to the paucity of information about the structure of naturally occurring eddies in the stratified ocean.

1. Introduction

This note was prompted by a suggestion that the vertical size of overturns in turbulent stratified flow in the ocean can be determined by gliders. This idea has led to a line of enquiry that reveals how little seems presently to be known about the structure of overturns in the ocean. The absence of such information leads to uncertainty in the estimates of the rate of dissipation of turbulent kinetic energy inferred indirectly from the size of glider-measured overturning scales. A distinction is drawn between overturns that move with the flow, like

1. School of Ocean Sciences, Bangor University, Menai Bridge, Anglesey LL595 AB, United Kingdom. Address for correspondence: 'Bodfryn', Glanrafon, Llangoed, Anglesey LL58 8PH, United Kingdom. ***email: oss413@sos.bangor.ac.uk***

Kelvin-Helmholtz billows, and those that propagate through the fluid, like those produced in convectively breaking internal waves. Attention is drawn to the possible differences in the estimates of overturns made from free-fall profilers, and those from gliders or AUVs that rise or sink through the water but move with a substantial horizontal component of motion relative to the flow, from moored profilers and from moored arrays or towed thermistor chains.

The vertical size of turbulent eddies containing regions of static instability (but not necessarily dynamic instability) where 'overturning' occurs and where the density of water increases upward, is commonly estimated by resorting a measured vertical density profile into a stable one in which density decreases upward everywhere, and finding the root mean square (rms) of the vertical displacements of fluid elements required to perform the resorting. The rms value provides a measure of the scale of overturn, usually termed the displacement scale, commonly denoted by L_T. (An intrinsic assumption in the reordering is that turbulence stirs a stratified fluid rapidly with relatively little molecular diffusion of the parameter, usually heat or salinity, that determines its density; Thorpe, 1977.) On average, L_T is found empirically to be proportional to the Ozmidov scale,

$$L_{Oz} = \varepsilon^{1/2}/N^{3/2}, \tag{1}$$

where ε is the rate of dissipation of turbulent kinetic energy per unit mass and N is the buoyancy frequency of the resorted density, with a constant of proportionality between L_T and L_{Oz} of about unity (Dillon, 1982; Peters *et al*., 1988; Wesson and Gregg, 1994; Ferron *et al.*, 1998). The Ozmidov scale characterizes the vertical scale of the largest eddies that overturn in a turbulent stratified fluid (Ozmidov, 1965).

Various instrumental means are available to provide measures of the vertical scales of overturning eddies. Of these, free-fall microstructure probes are perhaps the most reliable. Falling freely through the water, they attain a horizontal motion close to that of the surrounding water and consequently measure profiles of density through the water that are very close to vertical. Where density can be inferred from temperature (e.g., in freshwater lakes or in the ocean where there is a monotonic relationship between salinity and density) measurements of temperature are often used to infer displacement scales. Vertical arrays of moored thermistors (e.g.,van Haren and Gostiaux, 2010) or towed thermistor chains (e.g., Marmorino, 1987) can be used to infer the size of overturns, provided the separation between sensors is sufficiently small, typically less than 1 m.

A rough estimate of the magnitude of the Ozmidov scale, useful in guiding the depth resolution required for measurements in a particular area, may be derived using the Osborn (1980) formula for the vertical eddy diffusivity,

$$K_V = 0.2\varepsilon/N^2, \tag{2}$$

equation (1) then giving $L_{Oz} = (5K_V/N)^{1/2}$, which can be determined if historical data for K_V (typically about $10^{-5}\,\mathrm{m^2\,s^{-1}}$) and N are available. Provided their vertical speed is

much greater than the horizontal speed of the passing water, moored profiling instruments (e.g. Thorpe, 1977) or lowered CTDs may also provide vertical measures of overturns.

Can gliders be used to provide accurate estimates of vertical overturning scales? These bodies, about 2 m in length, generally move through the water at speeds of 0.2–1 m s^{-1} and at angles, α, to the horizontal of 14–45 deg (Eriksen, 2009); they do not move vertically through the water, but may, for example, measure the mean vertical separation of points over which the density measured along their path increases (or decreases) as they move upward (or downward) along their slanting path. The question then is: 'How do these slantwise measured vertical scales compare to those measured by a vertically profiling instrument?'

The answer evidently depends on α and the shape, and possibly the motion through the water, of the overturns. Three classes of overturns about which some information is available and that can be modeled in simple analytical ways are considered here: Kelvin-Helmholtz and Holmboe billows, coherent eddies in turbulent stratified waters, and convectively overturning internal gravity waves. These are addressed separately in the following three sections, and general conclusions are drawn in the final section. In a companion paper (Smyth and Thorpe, 2012) a more sophisticated model of K-H billows than that used here is adopted to estimate more accurately the displacement scales measured by gliders passing through them.

2. Kelvin-Helmholtz and Holmboe billows

Kelvin-Helmholtz (K-H) billows are fluid structures marking a stage of the transition from a laminar or relatively low turbulence regime to a turbulent regime in a stratified shear flow. Billows develop at sufficiently small values of the minimum gradient Richardson number, Ri, with their axes aligned in the direction of the vorticity vector of the mean flow, and they move at a speed close to that of the mean flow at the level where they form. Laboratory experiments in which K-H billows are produced on an interface between two fluids of differing density in relative motion (Thorpe, 1973) find that, before pairing of neighboring billows (if it occurs), their aspect ratio, b/a, taken as their height, $2b$, divided by their length, $2a$, measured normal to the axes of the billows (i.e., in the horizontal direction normal to the vorticity vector of the mean flow), decreases from about 0.5 to 0.06 as Ri at the onset of instability increases from 0.06 to 0.19. The overturning regions of the billows are of a roughly elliptical form with major axes that are horizontal. Pairing occurs mainly when Ri is significantly less than the canonical value, 1/4. The length of billows' crests, their 'transverse' scale, is typically about $8a$ before pairing between neighboring billows or some other along-crest disruption occurs, limiting the crest length (Thorpe, 2002). Billows formed by Holmboe instability observed in laboratory experiments, for example, by Thorpe (1968), Lawrence *et al.* (1991) and Strang and Fernando (2001), have aspect ratios of 0.2–0.3, and, like K-H billows, transverse scales (shown by Lawrence *et al.*) of about $8a$ prior to the development of three-dimensional instabilities. The billows occurring on a shallow flowing layer in Pawlak and Armi's (1998) laboratory experiments have an aspect ratio of about 0.5.

There appear to be no measurements of the transverse scale of naturally occurring billows in the sea or in lakes, and no clear evidence of billow pairing. The billows photographed by Woods (1968) in the Mediterranean seasonal thermocline have an aspect ratio, b/a, of about 0.5. Those measured using arrays of thermistors in Loch Ness by Thorpe *et al.* (1977) – although these have a structure resembling Holmboe instability - and Thorpe (1978) have aspect ratios of about 0.43 and 0.15, respectively. Billows observed by Marmorino (1987) using a towed thermistor chain in the seasonal thermocline of the Sargasso have an aspect ratio of about 0.2, although there is no certainty that the measured horizontal dimension (along the track of the vessel towing the chain) is normal to the vorticity of the mean flow. Van Haren and Gostiaux's (2010) billows measured by an array of 100 temperature sensors on a vertical mooring above the sloping side of the Great Meteor Seamount in the Canary Basin have an aspect ratio of about 0.15.

Overall, the aspect ratio of naturally-occurring billows appears to range from about 0.15 to 0.5. The transverse scales are presently unknown. What overturning scale might be inferred from a glider moving through a billow?

For simplicity, we shall first consider a glider moving through a single elliptical billow in a vertical plane normal to the billow axis (Fig. 1a), and intersecting the major axis of the ellipse, taken as the x-axis, in a point X at distance X from its center. We neglect the glider motion induced by the motion field of the billow or the mean shear. Although the billow will contain a spiraling density structure and the vertical density gradient may change sign within the billow, we disregard the complexity involved in accounting for this fine structure (it is considered by Smyth and Thorpe, 2012), and suppose that the overturning scale of the billow is simply given by its root mean square (rms) height. The vertical axis is z, and the ellipse is

$$x^2/a^2 + z^2/b^2 = 1, \tag{3}$$

while the glider path is $x = X + z\cot\alpha$. The glider therefore meets the elliptical edge of the billow at two locations, A and B, where $z = z_2$ and z_1, respectively, given by the roots of

$$(X + z\cot\alpha)^2/a^2 + z^2/b^2 = 1. \tag{4}$$

Hence solving the quadratic for z and subtracting the roots, the height of the billow observed by the glider is

$$z_1 - z_2 = 2ab\tan\alpha(b^2 + a^2\tan^2\alpha - X^2\tan^2\alpha)^{1/2}/(a^2\tan^2\alpha + b^2). \tag{5}$$

The roots of (4) are equal at two values of X (the points X_1 and X_2 in Figure 1a) when the glider is tangential to the billow ellipse: when

$$\begin{aligned} X = X_1, X_2 \text{ say}, &= \pm a(1 + (b/a)^2\cot^2\alpha)^{1/2} \\ &= \pm aq, \text{ say}, \end{aligned} \tag{6}$$

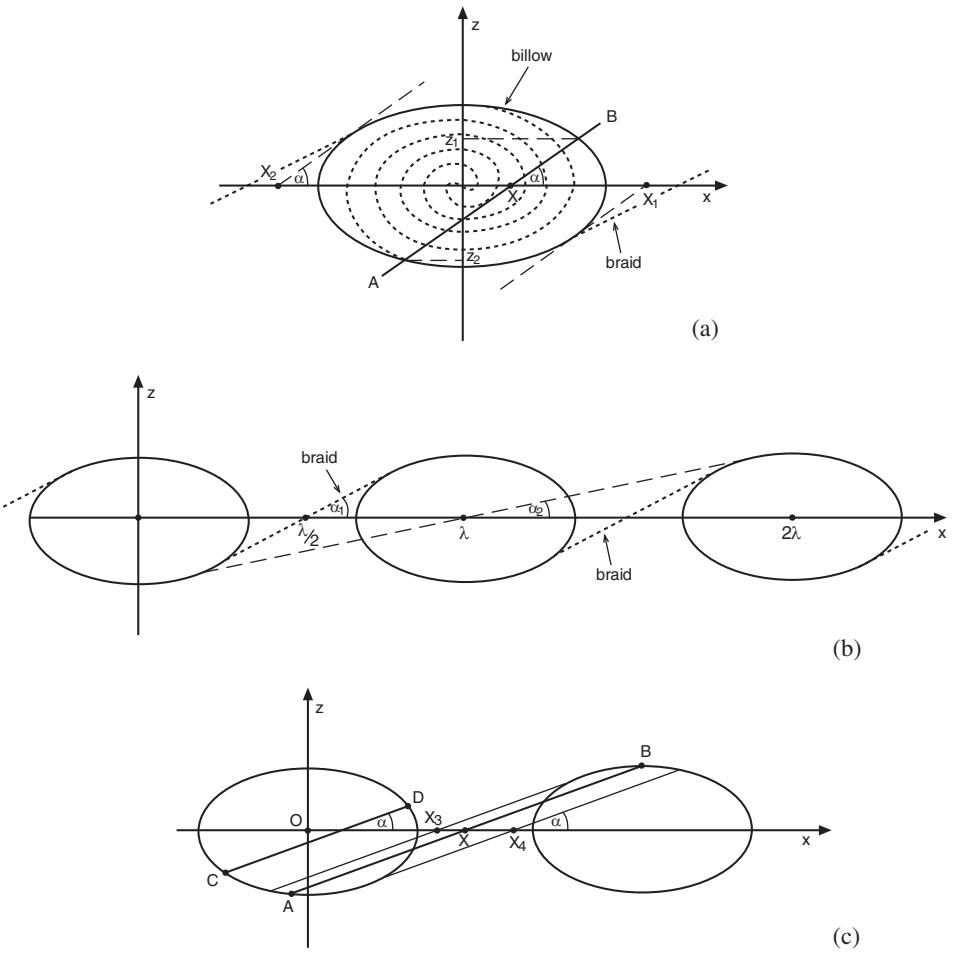

Figure 1. The approximately elliptical shape of billows. (a) The line AB represents the track of a glider, inclined to the horizontal at angle α, passing through a billow and measuring a vertical scale, $z_1 - z_2$. Tangents to the elliptical billow parallel to AB meet the major axis at points X_2 and X_1. (b) Intersection of glider paths with a train of billows. If $\alpha > \alpha_1$, equal to the slope of the braid between the two billows, the path intersects only one billow. If $\alpha_2 < \alpha < \alpha_1$ the path may intersect two billows while if $\alpha < \alpha_2$ three billows may be intersected. (c) A glider path, AB, intersecting two billows when $\alpha_2 < \alpha < \alpha_1$. The vertical distance between A and B gives the (local) apparent height of an overturn. Only when the point X where AB meets the major axis of the elliptical billows lies between X_3 and X_4 will a glider path intersect two billows. A single intersection is shown by the glider path CD.

where $q = (1+(b/a)^2 \cot^2 \alpha)^{1/2}$. The mean square billow height, ζ^2, observed by the glider passing repeatedly at inclination, α, through billows, is found by integrating $(z_1 - z_2)^2$ over the range of X from X_2 to X_1 (recalling that the overturning scale is zero when $X < X_2$

Table 1. Values of *Bf*, a measure of the 'error' involved in taking the glider overturn measurements, for representative values of glider inclination, α, and billow aspect ratio, b/a. The range $0.15 \leq b/a \leq 0.5$ is that of the billow shape in a vertical plane normal to the axes of the observed billow crests. The corresponding range in a vertical plane through the billow crests is 0.0375 to 0.125. The values of *Bf* are given by (8) except when $\alpha = 20$ deg. and $b/a = 0.5$ and glider paths may intersect two neighboring billows, when an amended calculation is as given in the Appendix.

	Aspect ratio, b/a				
α (deg)	0.0375	0.125	0.15	0.3	0.5
20	0.997	0.973	0.962	0.879	0.936
30	0.999	0.988	0.984	0.943	0.869
40	0.999	0.994	0.992	0.971	0.927

and when $X > X_1$) and dividing by the X range, taken as $-\lambda/2 < X < \lambda/2$, the range of x between the braids in Figure 1a, where λ is the billow wavelength and we have assumed $aq < \lambda/2$. Taking the square root gives the rms billow height measured along the glider path as

$$\xi = 4b[a/(3\lambda q)]^{1/2}. \tag{7}$$

The corresponding rms billow height measured by a vertically falling probe averaged over the range of X from $-\lambda/2$ to $\lambda/2$ is $4b[a/(3\lambda)]^{1/2}$, found from (7) in the limit as α tends to 90 deg. The ratio, *Bf*, of the glider-measured height to a vertical profiler measurement of the billow overturning scale (*Bf* consequently being a measure of the Bias function or error involved in taking the glider overturn measurements) is therefore

$$Bf = q^{1/2} = \{1 + [(b/a)\cot\alpha]^2\}^{-1/4}. \tag{8}$$

This is displayed in Table 1 for representative values of α and b/a. The measure of error, *Bf*, is less than unity and decreases – implying greater errors - as b/a increases at fixed α or as α decreases for fixed b/a; the errors become larger as the aspect ratio of the billows increases and as the glider angle decreases. Substantial underestimation of the overturning scale may occur but only for a billow with small aspect ratio or when the glider path is inclined at a small angle to the horizontal.

For comparison we consider measurements by a glider moving in a vertical plane *parallel* to the billow crests. The transverse extent of billows, the length of the billow crests, is taken from the laboratory observations as $8a$ (4 times the major axis of the billows) and it is supposed that the transverse section through the center of the billows is elliptical with aspect ratio, $b/4a$, one quarter of the previous value or a range of aspect ratios from 0.0375 to 0.125 for naturally-occurring billows. Values of *Bf* in Table 1 now lie between 0.97 and unity, implying relatively small errors in the measurement of the overturn scale.

Returning to glider paths in a vertical plane *normal* to the billow axis: (8) applies when $aq < \lambda/2$. When $aq > \lambda/2$, the glider path may intersect two or more billows in a train of billows, as shown in Figure 1b. The condition for such multiple intersections is that α is less than the slope of the braids between neighboring billows, which is roughly equal to $\tan^{-1}(b/a)$ (see Appendix). For a path to intersect more than one billow it is therefore necessary that $\alpha < \alpha_1 \approx \tan^{-1}(b/a)$; (8) is valid only for $\alpha > \alpha_1$. Because *Bf* in (8) decreases as α decreases, it has a minimum value at $\alpha = \alpha_1$ of $2^{-1/4} \approx 0.841$. Since the largest observed value of b/a is about 0.5, the largest value of α_1 is about 26.6 deg; when $\alpha = 20$ deg, multiple intersections will only be possible for billows with $b/a > 0.364$. The calculation of *Bf* when $\alpha < \alpha_1$ is outlined in the Appendix, and the value shown in Table 1 at $\alpha = 20$ deg., $b/a = 0.5$, accounts for the intersection of glider paths with a second billow. The value, $Bf = 0.936$, compares with a value, 0.767, given by (8) when the intersection with the second billow is ignored; accounting for intersection with a second billow leads to an increase in *Bf*.

As α decreases further below α_1, the glider path may intersect more than two billows but the analytical estimates of *Bf* become unrealistic: very long trains of billows of uniform size do not occur naturally.

At a later stage in the transition from laminar flow to turbulence driven by K-H instability, after the billows have amalgamated to form a horizontally homogeneous layer of turbulent flow, the vertical overturning scale will become almost independent of α with $Bf \approx 1$. Some slight differences in values of *Bf* at small positive and negative α may, however, exist as a consequence of the remaining, slightly tilted, striated structure of the density field (e.g., see Thorpe, 1971; Figs. j–n).

3. Coherent eddies in turbulent flow

We are aware of no studies of the detailed structure of the density within eddies in turbulent stratified shear flows that might be used to obtain precise measures of the vertical scales of overturns made along the inclined glider paths. There are, however, some, but few, observations of the autocorrelation structure of the thermal field that provide some indication of the size and shape of coherent eddies. Keller and Van Atta (2000) measured turbulent temperature fluctuations with a vertical array of sensors in a uniformly and thermally stratified, uniform shear flow downstream of a grid in the laboratory. They present isocontours of the autocorrelations of temperature fluctuations in a vertical plane orientated in the downstream direction in mean flows with Richardson numbers of 0.015, 0.095 and 0.5. The roughly elliptical contours with aspect ratios, b/a, of about 0.45 are tilted upward by angles, β, (Fig. 2) of 35, 31 and 20 deg, respectively, in a direction consistent with the imposed shear. No correlation values transverse to the flow are given. Detailed temperature correlations have also been obtained in freshwater lakes, although only in the near-surface mixed layer. Ozen *et al*. (2006) made measurements in Lake Geneva from a submersible carrying a vertical and transverse array of thermistors. The autocorrelations in

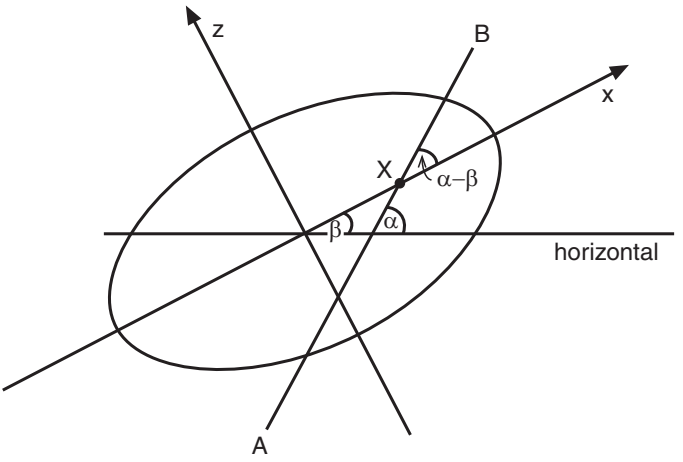

Figure 2. An elliptical isocontour of the autocorrelation of temperature fluctuation in a vertical, $x-z$, plane. The aspect ratio is b/a and the major axis of the isocontour of length $2a$ is inclined at an angle β to the horizontal. The line AB represents the track of a glider, inclined to the horizontal at angle α, passing through the typical structure of a coherent eddy defined by the isocontour.

the along-track direction (up-wind) are inferred using the Taylor hypothesis. The isocontours in the vertical plane orientated along-track have an elliptical structure with aspect ratio of about 0.5–0.8 and are tilted with $\beta \approx 60$ deg. (Similarly tilted structures are observed using a three-dimensional moored array of thermistors in Loch Ness by Thorpe and Hall (1977). The coherent structures advect through the stationary array with the mean flow.) In the transverse y direction the correlation is greater than in the along-track direction, the y-distance over which the correlation coefficient equals 0.6 being, for example, about 1.6 times the along-track distance. The thermal structures result from the process of entrainment of cold water from the thermocline into the mixed layer and have some similarity to those produced by Holmboe instability.

Supposing these coherent structures represent the average structure of overturns, we may, as in Section 2, compare the vertical scales observed along glider tracks at angles, α, to the horizontal, i.e., at an angle, $(\alpha - \beta)$, to the major axis of the elliptical isocontours (Fig. 2), taking averages over one wavelength, λ. Following the analysis of Section 2 but putting α equal to $\alpha - \beta$ and projecting the length AB onto the new vertical direction, we find that the ratio, *Bf*, of the glider to the vertical profiler measurement of the billow overturning scale, is given by

$$Bf = |\sin\alpha|^{1/2}\{[\cos^2\beta + (b/a)^2\sin^2\beta]/[\sin^2(\alpha-\beta) + (b/a)^2\cos^2(\alpha-\beta)]\}^{1/4}. \quad (9)$$

This model contains a single billow, but is comparable to the case of an infinite train of billows considered in Smyth and Thorpe (2012) provided that the glider trajectory does not

Table 2. Values of *Bf*, a measure of the 'error' involved in taking the glider overturn measurements, for representative values of glider inclination, α, and turbulent eddy aspect ratio, b/a, and inclination, β, of its major axis, with values taken from top: Keller and Van Atta (2000) with aspect ratio, $b/a = 0.45$; and below: Ozen *et al.* (2006) with $\beta = 60$ deg. (Values of *Bf* found using (9) with $b/a = 0.43$ and for $\beta = -20$ deg are given by Smyth and Thorpe, 2012, Fig. 5.)

	β (deg)	
α (deg)	20	35
20	0.851	0.762
30	1.000	0.970
40	1.061	1.099
−20	0.669	0.585
−30	0.762	0.681
−40	0.827	0.740
α (deg)	aspect ratio, b/a	
	0.5	0.8
20	0.550	0.574
30	0.706	0.707
40	0.856	0.815
−20	0.479	0.542
−30	0.575	0.653
−40	0.656	0.743

encounter neighboring billows, i.e., if $\lambda > 2a \sin(\beta-\alpha)[1+(b/a)^2 \cot^2(\beta-\alpha)]^{1/2}/|\sin\alpha|$. This equation for *Bf* reduces to (8) when $\beta = 0$ and equals 1 if $\alpha = 90$ deg. Values of *Bf* are shown in Table 2 for representative values of α, β and b/a. Although generally of order unity implying relatively small errors, values may exceed 1 and are sometimes small, implying relatively large errors may occur when α is small.

4. Convectively breaking internal gravity waves

Although a special case, two-dimensional internal gravity waves propagating in the (x, z) plane through a fluid of uniform buoyancy frequency, N, provide a description of the modulated structure observed in waves passing through the thermocline (e.g., Lazier and Sandstrom, 1978). Their presence is shown to lead to the possible detection of false overturns. There is the substantial advantage that, even when overturning, the waves can be expressed exactly by the simple set of equations for the horizontal and vertical components of velocity:

$$u = (am\sigma/k)\cos(kx + mz - \sigma t),\ w = -a\sigma\cos(kx + mz - \sigma t), \tag{10}$$

density:

$$\rho = \rho_0\{1 - N^2 g^{-1}[z - a\sin(kx + mz - \sigma t)]\}, \tag{11}$$

with dispersion relation:

$$\sigma^2 = k^2 N^2/(k^2 + m^2), \tag{12}$$

where a is now the wave amplitude (the amplitude of isopycnal surfaces), (k, m) is the wavenumber vector, σ is the wave frequency and g is the acceleration due to gravity. For simplicity the effects of the Earth's rotation are ignored. Isopycnal surfaces are shown in Figure 3. The vertical density gradient

$$\partial\rho/\partial z = \rho_0 N^2 g^{-1}[am\cos(kx + mz - \sigma t) - 1], \tag{13}$$

is greatest on the lines

$$kx + mz - \sigma t = 2n\pi, \tag{14}$$

where n is an integer. If the slope of the waves, $s = am$, is greater than 1, (13) implies that near these lines $\partial\rho/\partial z > 0$, and the isopycnals overturn as in Figure 3b resulting in regions that are statically unstable (shown hatched) surrounding the lines (14).[2] The convectively breaking internal wave equations, (10)–(12) with $s > 1$, provide a simple mathematical description of overturns. Unlike the billows or coherent structures in turbulent stratified shear flows, the overturning regions, propagate through the stratified fluid at phase speed $\underline{c} = (\sigma/K^2)(k, m)$, where $K^2 = k^2 + m^2$, and with group velocity $\underline{c}_g = [mN^2/(\sigma K^4)][km, -(k^2 + l^2)]$ inclined at an angle θ to the horizontal as shown in Figure 3. This angle, θ, has values between 0, for low frequency waves, and 90 deg for waves of frequency close to the buoyancy frequency. Waves radiating from turbulent regions, e.g., the upper ocean mixed layer, are found to have $\theta \sim 45$–60 deg (Linden, 1975; Sutherland and Linden, 1998).

The height of the overturning scales, taken as the vertical size of the statically unstable regions at the onset of convective breaking in internal gravity waves, is now examined. A glider is allowed to have a velocity component in the y direction normal to the plane of propagation of the waves, so that its velocity relative to the water through which it is rising can be written $(-V\cos\alpha\cos\phi, V\cos\alpha\sin\phi, V\sin\alpha)$, where α is the inclination to the horizontal negative x axis (Fig. 4) and ϕ is an azimuthal direction, the angle between the projection of the glider path onto the horizontal and the negative x direction.

2. In their abstract, Liu *et al.* (2010) state "Isopycnal overturning is induced at a local wave steepness of $s_c = 0.75$–0.79, which is below the conventional threshold of $s = 1$." The parameter, s, in that work is, however, taken as the slope of internal waves being forced at the upper boundary of a stratified domain. The wave slope is modulated with distance from the boundary, leading to regions of overturn and mixing. Liu states in private correspondence (2011) that the word "local" in the quoted sentence in their abstract should be deleted.

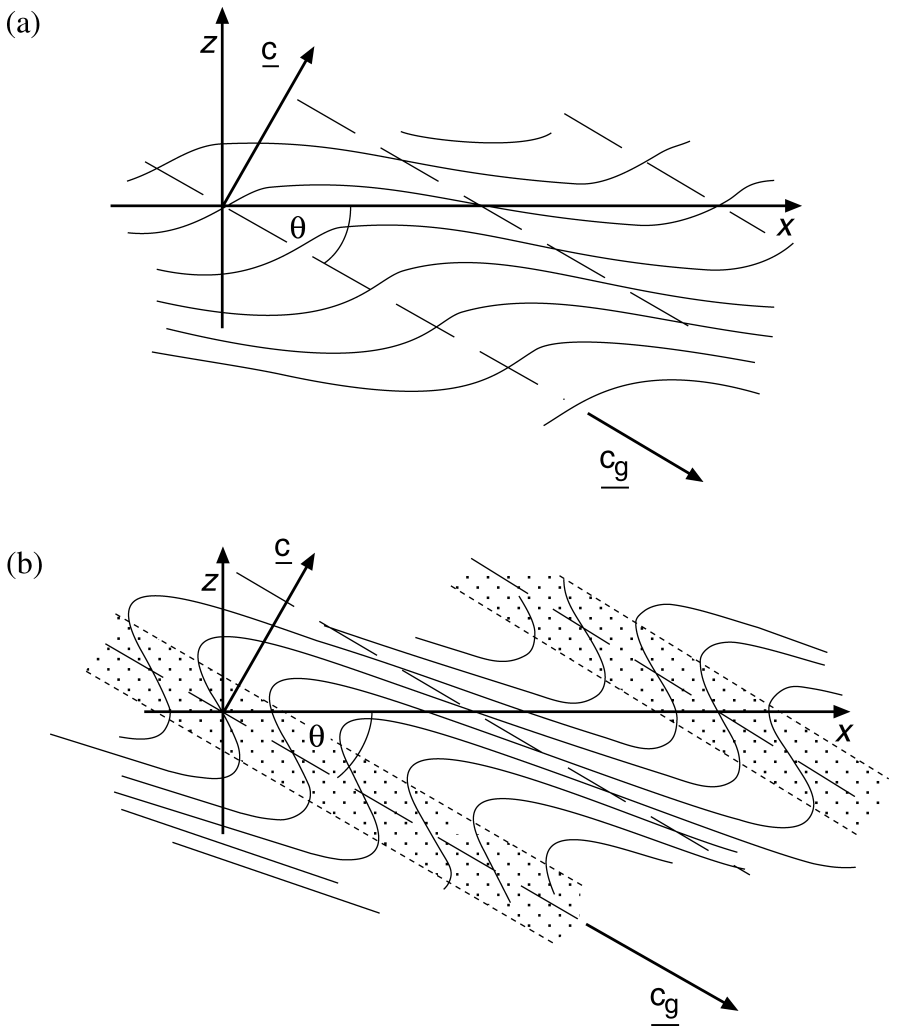

Figure 3. Isopycnal surfaces of internal gravity waves travelling through a uniformly stratified fluid with (a) $s < 1$ and (b) $s > 1$. Three surfaces of constant phase are shown by the dashed lines. The waves in (b) are statically unstable in the hatched regions. The group velocity, $\underline{c}_g$, is inclined to the horizontal at an angle θ. (From Thorpe, 1994.)

We may consider three different Cases of increasing complexity and approach to reality: (a) in which the glider moves at a constant speed, V, and upward inclination, α, through stationary waves (appropriate when $V \gg c = \sigma/K$; invoking symmetry, we select an upward glider path without loss of generality); or (b) through moving waves; or (c) in which it moves at a speed V and inclination, α, relative to the water that moves with the wave-induced speeds (10). In each case we fix the origin and the time $t = 0$ at the position

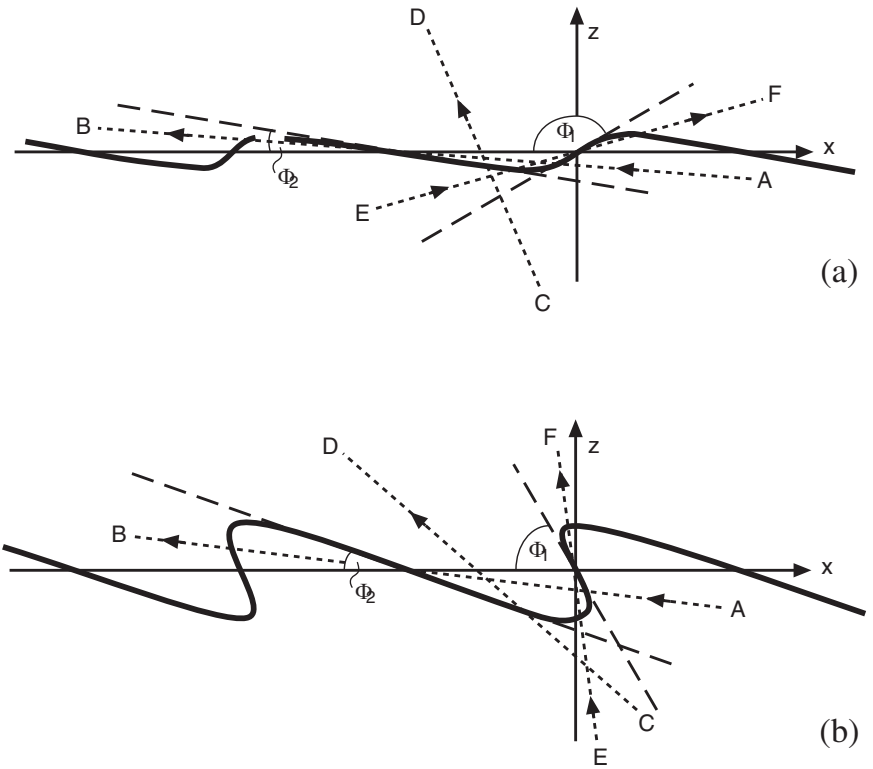

Figure 4. The slope angles, Φ_1 and Φ_2, of an isopycnal surface distorted by the presence of internal gravity waves as shown in Figure 3 with (a) statically stable waves with $s < 1$, and (b) overturning waves with $s > 1$. Glider tracks when $V \gg c$, when the wave field is effectively frozen, are also shown by the straight lines, AB, CD and EF. The angle α is the inclination of the glider track to the negative x-axis. Track AB, with $\alpha < \Phi_2$, intersects the isopycnal surface several times and will consequently measure a density gradient along its path that changes sign with, therefore, apparent overturns, whether or not the wave is overturning. A glider moving along track CD with $\Phi_2 < \alpha < \Phi_1$ intersects the isopycnal surface only once: the density therefore decreases monotonically, with no apparent overturns. 'Real overturns' are measured by tracks like EF in part (b) with $\Phi_1 < \alpha < 90$ deg when $s > 1$. Apparent overturns may be detected as on track EF as in part (a) provided 180 deg $> \alpha > \Phi_1 > 90$ deg (i.e., when $s < 1$ and no overturning is present).

where the glider passes through the surface given by (14) with n chosen there to be zero. (In traversing the density field, the glider will generally somewhere cross such a surface, and the origin is chosen at the point of its intersection.)

We define two angles, Φ_1 and Φ_2, related to the wave slope. These are shown in Figure 4. At time $t = 0$, the equation for the isopycnal surface where $\rho = \rho_0$ is $z = \eta(x)$ and where, from (11),

$$\eta = a \sin(kx + m\eta). \tag{15}$$

The gradient of the isopycnal surface, $d\eta/dx$, is given by

$$d\eta/dx = a(k + md\eta/dx)\cos(kx + m\eta), \tag{16}$$

so at $\eta = x = 0$ (zero phase),

$$d\eta/dx = ak/(1 - s) = s\tan\theta/(1 - s), \tag{17}$$

using $k = m\tan\theta$ and $s = am$. The inclination of the surface to the negative x direction is $\Phi_1 = \tan^{-1}[s\tan\theta/(s - 1)]$, which is positive implying the angle Φ_1 is <90 deg (but > θ), if $s > 1$ as shown in Figure 4b. Where the wave displacement, $\eta = 0$ at $kx = \pi$ (180 deg phase), the gradient of the isopycnal surface is

$$d\eta/dx = -ak/(1 + s) = -s\tan\theta/(1 + s). \tag{18}$$

The inclination of the isopycnal surface to the negative x direction is therefore $\Phi_2 = \tan^{-1}[s\tan\theta/(s+1)]$, as in Figure 4a. Since $s > 0$, the angle Φ_2 is less than θ and therefore $< \Phi_1$.

If, in moving through a frozen wave field, the glider angle, α, $< \Phi_2$ or if $\alpha > \Phi_1$, its path will cross some isopycnal wave surfaces more than once and hence it will record an along-track density gradient that changes sign even though there is no overturning (i.e., when $s < 1$); as illustrated in Figure 4, such false overturns may be recorded by gliders moving through an internal wave field.[3] The condition for false overturns, $\alpha < \Phi_2$, is satisfied only if $0 < \alpha < \theta \leq 90$ deg, and if $s > 1/[\tan\theta/\tan\alpha - 1]$. When $s < 1$, the condition $\alpha > \Phi_1$ (Fig. 4a) for a false overturn is found only when $180 > \alpha(\text{deg}) > 90$ and $s > 1/(1 - \tan\theta/\tan\alpha)$ (an expression which is <1 since $\tan\alpha < 0$). If $s > 1$, the overturn with $\alpha > \Phi_1$ (Fig. 4b) will be observed if $90 \leq \alpha(\text{deg}) < 180$ or at smaller α when $s > 1/(1 - \tan\theta/\tan\alpha)$.

Two measures of the size of overturns are estimated and compared. An 'overturning scale' is defined as the vertical distance, but measured along the glider track, over which the upward vertical density gradient measured by the moving glider is positive. A 'displacement scale,' L_T, is found by the conventional reordering of the observed density profile (but again measured along the glider track) into a stable one and integrating the displacements of fluid elements required to do this. Both measures are normalized by dividing by $2a$. We shall find, however, that in Case (c) the choice of seeking a range in the vertical, Z, measured along a glider track in which ρ increases with Z can lead to some anomalous and non-meaningful estimates of the size of overturns.

a. A vertically moving measuring probe in a stationary wave field

The overturning scale of the internal wave measured by a probe rising vertically through a stationary wave field, Case (a), can be found by putting $x = t = 0$ in (13). We have

3. Such false overturns are foreseen by Thorpe (1977; his Fig. 7).

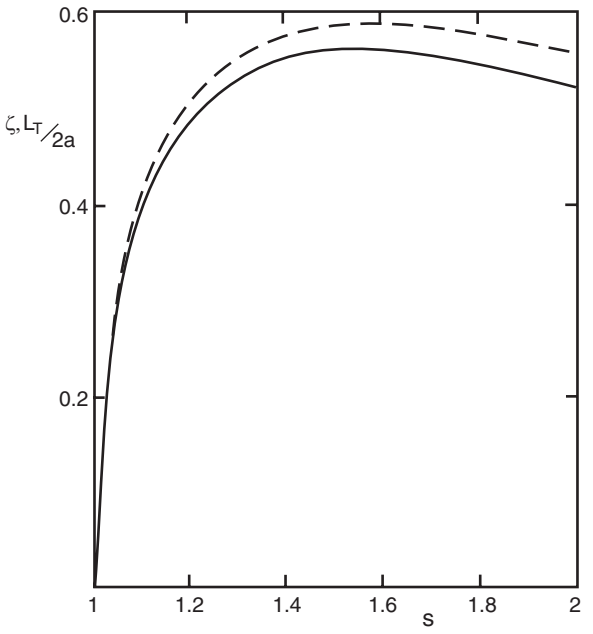

Figure 5. The rms displacements, L_T, (dashed line) resulting from reordering the density profile, $\rho = \rho_0\{1 - N^2 g^{-1}[z - a\sin(mz)]\}$ over the vertical region within which convective instability may occur when $s > 1$, normalized with $2a$, and the scale, ζ, of the statically unstable region (full line), given by (19).

$am\cos(mz) = 1$ at $\partial\rho/\partial z = 0$, and since when $s > 1$, $\partial\rho/\partial z > 0$ at $z = 0$, the nondimensional height of the overturning region, the true overturning scale of the internal wave, is given by

$$\zeta = 2z/2a = (1/s)\cos^{-1}(1/s). \tag{19}$$

Values are shown, together with the displacement scales, L_T, in Figure 5. Remarkably, ζ and L_T do not depend on θ. The two metrics are different; the conventionally estimated displacement, L_T, scale differs from that determined by measuring the heights of statically unstable regions. Their ratio provides a correction that may be applied to derive L_T from values of ζ measured by a glider moving along tracks inclined to the vertical through waves with effective slopes, s, provided that the form of the equation for density remains the same as in (11), i.e., containing a constant and a linear term plus a sinusoidal function of location, z or Z, as it does in Cases (a) and (b). Because of the relative motion of the waves in Cases (b) and (c), the measured overturning and displacement scales when $\alpha = 90$ deg might be expected to differ from the actual overturn scales of the frozen wave field. We later consider whether this is so.

Case (a); stationary waves

Without loss of generality (by taking $t = 0$ as a glider path passes through one of the long-dashed lines in Fig. 3), we can consider a glider track passing through the origin, $x = z = 0$ at time $t = 0$. Taking the along-track distance moved by the glider as $D(= Vt)$, its location at time t is

$$x = -D\cos\alpha\cos\phi,\ y = D\cos\alpha\sin\phi,\ z = D\sin\alpha. \tag{20}$$

From (11) but putting $t = 0$ in this equation because the wave is frozen, the glider therefore records a density

$$\begin{aligned}\rho &= \rho_0\{1 - N^2 g^{-1}[D\sin\alpha - a\sin(mD\sin\alpha - kD\cos\alpha\cos\phi)]\},\\ &= \rho_0\{1 - N^2 g^{-1}[D\sin\alpha - a\sin((D\gamma/a)\sin\alpha)]\},\end{aligned} \tag{21}$$

using $k = m\tan\theta$, where $\gamma = s(1 - \cos\phi\tan\theta/\tan\alpha)$. If $\cos\phi = \tan\alpha/\tan\theta$ then $\gamma = 0$ and the sine term in (21) vanishes, so the density gradient sampled by the glider moving with directions (α, ϕ) is constant. In general, however, the along-track density gradient is zero when $d\rho/dD = 0$, or when the vertical location of the glider is given by $z = z_0$ and $D = D_0$ where

$$z_0/a, = D_0\sin\alpha/a, = (1/\gamma)\cos^{-1}(1/\gamma). \tag{22}$$

Real values of $D_0\sin\alpha$ are found only when $|\gamma| > 1$. This condition is satisfied for some ϕ provided α does not lie between Φ_2 and Φ_1. The apparent height of overturns is then $2D_0\sin\alpha$. (Alternatively, a glider track assigned through $x = \pi/k$, $z = 0$ at $t = 0$ leads to $D_0\sin\alpha/a, = (1/\gamma)\cos^{-1}(-1/\gamma)$ and gives an apparent overturn height $2|D_0|\sin\alpha$ when $\gamma < 0$.) Nondimensionalizing with the wave amplitude, a, the actual height of overturns is found by putting $\alpha = 90$ deg, giving $\gamma = s$ and $\zeta = 2D_0\sin\alpha/2a = (1/s)\cos^{-1}(1/s)$ as in (19).

To provide examples, we suppose that the glider track lies in the $x - z$ plane (so $\phi = 0$) in which the internal wave is traveling. If $\alpha > \theta$, then $\alpha > \Phi_2$, and there are no tracks like those shown by the lines AB in Figure 4, and no corresponding solutions for ζ for false, or unreal overturns. If, however, $\alpha > \Phi_1$, with s > 1, real values of ζ are found corresponding to track EF in Figure 4b. When $\tan\theta = 0.125$ ($\theta = 7.1$ deg) there are no false overturns and no solutions for ζ if $\alpha > 7.1$ deg, but real overturns are possible with real values of ζ when $s > 1$ provided α and s are large enough, as shown e.g., in Figure 6a. Similarly if $\tan\theta = 1.0$ ($\theta = 45$ deg), false overturns are observed when for $\alpha < \Phi_2$, or when $s > [(\tan\alpha)^{-1} - 1]^{-1}$, even when $s > 1$ and real overturns are present in the internal wave (Fig. 6b). For this value of θ, $\Phi_1 = \tan^{-1}[s/(s-1)] > 63.4$ deg if $1 < s \le 2$ (the range of $s > 1$ shown in Fig. 6b); there are therefore no glider paths, EF in Figure 4b, with $\alpha > \Phi_1$, that intersect the overturning region of the internal wave. Corresponding values of ζ, when the glider path is normal to the plane of the internal wave ($\phi = 90$ deg), are shown by dashed lines in Figure 6a and b. In this case ζ is independent of α since $\gamma = s$.

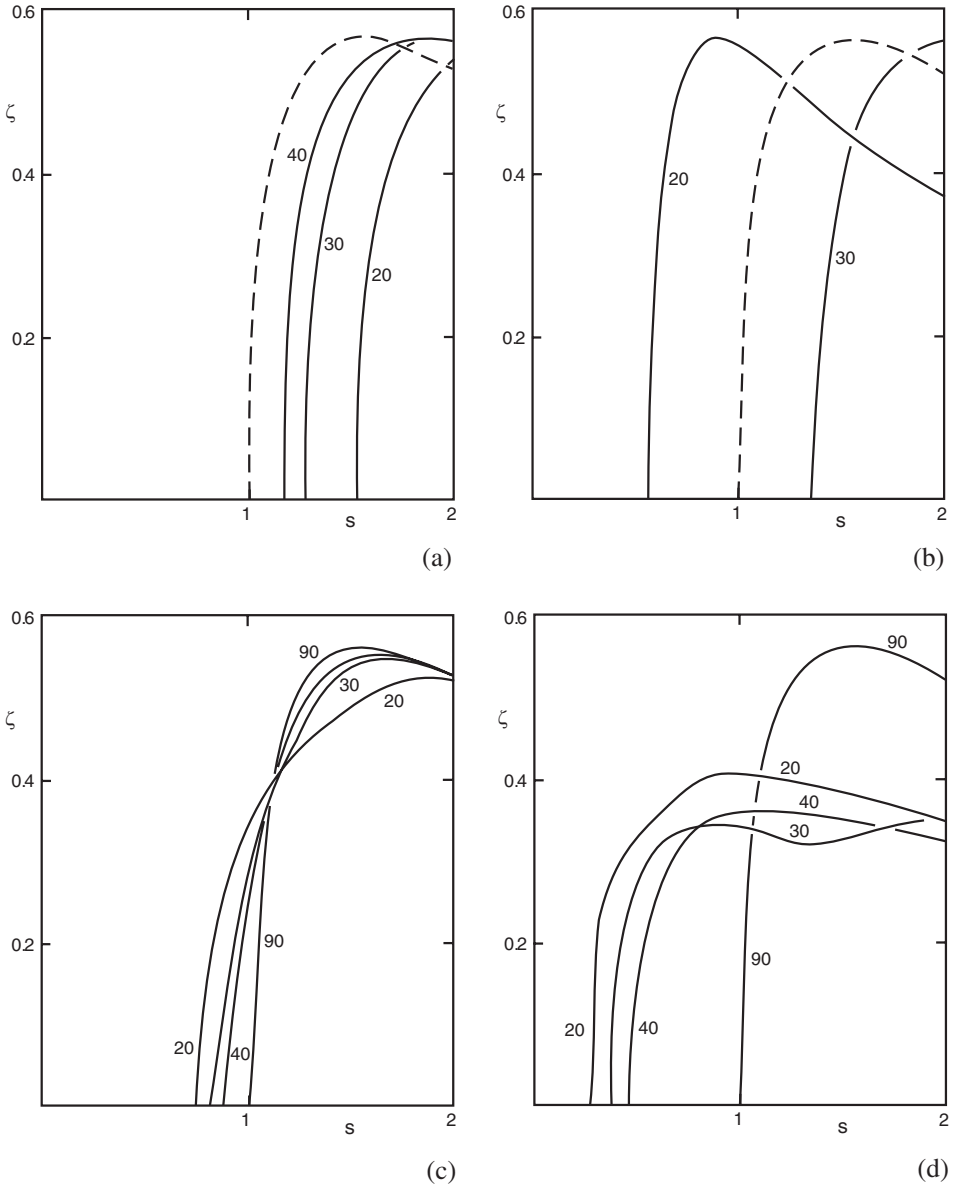

Figure 6. Case a: The overturning scales, ζ, measured by a glider moving at speed, V, at an angle of inclination to the horizontal, $\alpha, = 20$, 30, 40 and 90 deg through stationary internal waves of steepness, s. (a): azimuthal angle, $\phi = 0$ (full lines) and $\phi = 90$ deg (dashed line) when $\tan\theta = 0.125$ ($\theta = 7.1$ deg); (b): $\phi = 0$ (full lines) and $\phi = 90$ deg (dashed line) when $\tan\theta = 1.0$ ($\theta = 45$ deg). (If $\alpha = 40$ deg, solutions for ζ are possible only if $s > 5.22$). In (c): $\tan\theta = 0.125$ ($\theta = 7.1$ deg), and (d): $\tan\theta = 1.0$ ($\theta = 45$ deg) the rms overturning scales are averaged over the azimuthal angle ϕ of the glider direction.

Generally the direction of a glider track relative to that of an internal wave will not be known. Supposing that a track is adopted so that the glider repeatedly samples a wave from differing directions, ϕ, we can estimate the rms apparent overturn scale measured as the glider moves at an angle, α, and now sampling the wave field from *all* azimuthal directions, ϕ. The rms overturn scale is found by (numerically) integrating ζ from $\phi = 0$ to $\phi = 180$ deg. The nondimensionalized, rms, apparent overturning scales given by (22) and calculated in the depth range $-\pi/2 < mz < \pi/2$ of a single internal wave are shown in Figure 6, c and d. The (real) overturning scales, given by $\alpha = 90$ deg, are seen to be overestimated at $\alpha = 20$, 30 and 40 deg in Figure 6 in the range $1/(1 + \tan\theta/\tan\alpha) < s < 1$ and in a range where $1 < s < \sim 1.1$, and underestimated at greater values of s. Although not shown here, the glider-measured overturning scales are close to the real scales when s exceeds 1.2 and θ is small, specifically when θ is less than about $\tan^{-1}(0.2\tan\alpha)$.

Case (b); propagating waves

Retaining the time, t, in (11), so allowing the internal wave to propagate, and writing $t = D/V$, we find the density measured by the glider as a function of along-track distance, D:

$$\begin{aligned}\rho &= \rho_0\{1 - N^2 g^{-1}[D\sin\alpha - a\sin(mD\sin\alpha - kD\cos\alpha\cos\phi - cmD\sec\theta/V)]\},\\ &= \rho_0\{1 - N^2 g^{-1}[D\sin\alpha - a\sin(D\gamma\sin\alpha/a)]\},\end{aligned} \tag{23}$$

where $\gamma = s[1 - \cos\phi\tan\theta/\tan\alpha - (c/V)/(\sin\alpha\cos\theta)]$ and the relations $c = \sigma/K$ and $k = m\tan\theta$ have been used. As in Case (a), the density gradient is constant in particular directions, those in which $\gamma = 0$, i.e., when $\cos\phi = (\tan\alpha/\tan\theta)[1 - (c/V)/\sin\alpha\cos\theta]$.

The rate of change in density along the glider track, $d\rho/dD$, is zero where $D = D_0$ with

$$D_0\sin\alpha = (a/\gamma)\cos^{-1}(1/\gamma). \tag{24}$$

Values of $\zeta = 2D_0\sin\alpha/2a$, when the azimuth angle, ϕ, $= 0$ or 90 deg, and $\tan\theta = 0.125$ and 1.0 are shown in Figure 7, a and b, when $c/V = 0.2$. As in Case (a), there are no solutions for ζ, and no overturns, false or real, found when $s < 1$ and $\tan\theta = 0.125$. However ζ now depends on α when $\phi = 90$ deg. The smallest values of s at which solutions for ζ are found are listed in the figure caption. For comparison, examples of the nondimensionalized rms apparent overturning scales, ζ, integrated over the azimuthal directions, ϕ, are shown in Figure 7, c and d, for $c/V = 0.2$. Although values at $s < 1$ are similar to those of Figure 6, c and d, when $c/V = 0$, the apparent overturning scales are generally reduced when s exceeds about 1.2. When $\alpha = 90$ deg, corresponding to the trajectory of a freely rising probe, the parameter γ is equal to $s[1 - (c/V)/\cos\theta]$, and

$$\zeta = 2D_0\sin\alpha/2a = \{1/[s[1 - (c/V)/\cos\theta]\}\cos^{-1}\{1/[s(1 - (c/V)/\cos\theta)]\}. \tag{25}$$

Comparing this to (19) we see that a probe in free-fall through the propagating wave field 'sees,' or measures, waves with effective slopes, $s[1 - (c/V)/\cos\theta]$, that differ from their real slopes, s. The cut-off at wave slopes found at $s = 1$ in Figure 5 now occurs at

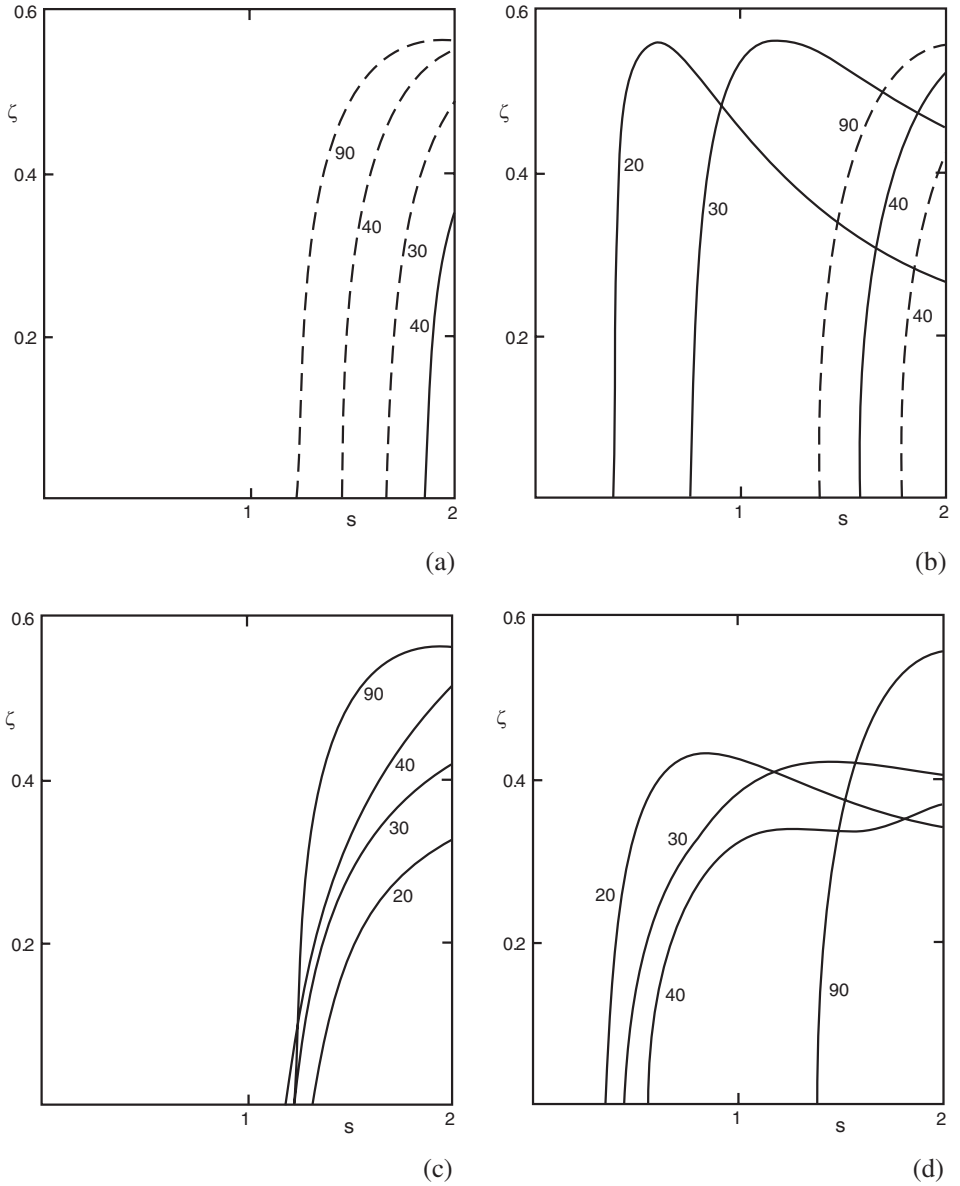

Figure 7. Case b: The overturning scales, ζ, measured by a glider moving at speed, V, with $c/V = 0.2$, at various labelled angles of inclination to the horizontal, α, through propagating internal waves of steepness, s, when the glider's motion is not affected by the motions induced by the waves. (a): azimuthal angle, $\phi = 0$ (full lines) and $\phi = 90$ deg (dashed lines) when $\tan\theta = 0.125$ ($\theta = 7.1$ deg). (When $\phi = 0$ and $\alpha = 20$ and 30 deg, s must exceed 14.9 and 2.63, respectively, for real values of ζ; and when $\phi = 90$ deg and $\alpha = 40$ deg, s must exceed 2.43 for real ζ.) (b): $\phi = 0$ (full lines) and $\phi = 90$ deg (dashed line) when $\tan\theta = 1.0$ ($\theta = 45$ deg). (If $\phi = 90$ deg and $\alpha = 20$ deg and 30 deg, s must exceed 5.78 and 2.30, respectively, for real ζ.) The rms overturning scales are averaged over the azimuthal angles, ϕ, of the glider direction relative to the x-z plane of the internal waves in (c) $\tan\theta = 0.125$ ($\theta = 7.1$), and (d) $\tan\theta = 1.0$ ($\theta = 45$ deg).

$s = [1 - (c/V)\cos\theta]^{-1} > 1$. For example, when $c/V = 0.2$, as in Figure 7, overturns for a vertically moving probe, $\alpha = 90$ deg, are only detected in waves with $\tan\theta = 0.125$ when their slopes exceed about 1.25.

Case (c); the glider track perturbed by internal waves

The oscillatory paths of particles in the internal waves are along straight lines parallel to the group velocity and therefore inclined at angle θ to the horizontal. Ignoring the time delays involved in accelerating the glider to conform to the wave induced motion, its motion when at a location (X, Y, Z) at time, t, is given by the sum of the wave motion, (10), and the relative glider motion:

$$dX/dt = (s\sigma/k)\cos(kX + mZ - \sigma t) - V\cos\alpha\cos\phi, \tag{26a}$$

$$dY/dt = V\cos\alpha\sin\phi, \tag{26b}$$

$$dZ/dt = -a\sigma\cos(kX + mZ - \sigma t) + V\sin\alpha. \tag{26c}$$

Adding k times (26a) and m times (26c) and integrating:

$$kX + mZ = Vt(m\sin\alpha - k\cos\alpha\cos\phi), \tag{27}$$

taking $X = Y = Z$ at $t = 0$. Substituting in (26c) and integrating:

$$Z = -(a/\Psi)\sin(\sigma\Psi t) + Vt\sin\alpha, \tag{28}$$

where $\Psi = [(V/\sigma)(m\sin\alpha - k\cos\alpha\cos\phi) - 1] = [(\sin\alpha\cos\theta - \cos\alpha\sin\theta\cos\phi)/(c/V)] - 1$. Expressions for the glider trajectory, X using (27) and (28), Y obtained by integrating (26b) and Z from (28), are now given in parametric form in terms of time, t. The term $\sin(\sigma\Psi t)$ introduced in (28) represents the perturbation of the wave field on the glider motion, Doppler shifted in frequency as a result of the glider motion through the waves. The density measured by the glider is found by substituting (27) and (28) into (11):

$$\rho = \rho_0\{1 - N^2 g^{-1}[Vt\sin\alpha - (a(1 + \Psi)/\Psi)\sin(\sigma\Psi t)]\}. \tag{29}$$

The time derivative of the density observed by the glider, $d\rho/dt$, is zero when

$$\begin{aligned}\sigma\Psi t &= \cos^{-1}\{V\sin\alpha/[a\sigma(1 + \Psi)]\} \\ &= \cos^{-1}\{1/[s(1 - \tan\theta\cos\phi/\tan\alpha)]\}, = \Omega \text{ say},\end{aligned} \tag{30}$$

or when, from (28), at glider location $Z = Z_0$ where

$$\begin{aligned}Z_0/a &= \{(V/\sigma a)\Omega\sin\alpha - \sin\Omega\}/\Psi \\ &= \{\Omega\sin\alpha\cos\theta/[s(c/V)] - \sin\Omega\}/\Psi.\end{aligned} \tag{31}$$

The parameter Ψ, is zero and Z/a in (31) tends to infinity when azimuth directions are given by $\cos\phi = \tan\alpha/\tan\theta - (c/V)/(\sin\theta\cos\alpha)$. For these values of ϕ, dZ/dt and

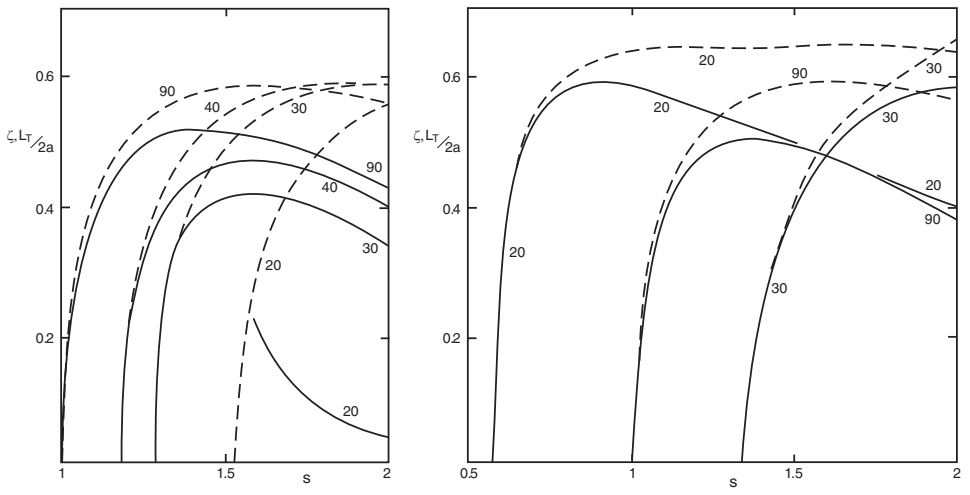

Figure 8. Case c: The normalized rms overturning scales, $\zeta = Z_0/a$ (full lines), and the rms displacements, $L_T/2a$ (dashed lines) measured by a glider moving at speed, V, with $c/V = 0.2$, at an angles of inclination to the horizontal, α, = 20, 30, 40 and 90 deg through propagating internal waves of steepness, s, with (a) $\tan\theta = 0.125$ ($\theta = 7.1$) and (b) $\tan\theta = 1.0$ ($\theta = 45$ deg) when the glider moves in the plane of the waves ($\phi = 0$) and the glider's velocity is affected by the motions induced by the waves.

$d\rho/dZ$ are constant. Small deviations from this azimuthal direction are found to lead to large apparent overturning scales, and for this reason integration is not made over ϕ in this Case.

Symmetry implies that in many cases (but see below) the apparent height of an overturn is $2Z_0$, the density increasing from $-Z_0$ to Z_0, and the normalized overturning scale is $\zeta = 2Z_0/2a$. Figure 8 shows examples of the normalized overturning scales, ζ, for glider tracks in the plane of the waves, $\phi = 0$, calculated in the range $-\pi/(2\sigma\Psi) < t < \pi/(2\sigma\Psi)$ of one Doppler shifted period, at various inclinations, α, to the horizontal. The figure also shows $L_T/2a$, the rms displacements divided by $2a$. Real solutions for Ω are found from (30) only when

$$|s(1 - \tan\theta/\tan\alpha)| \geq 1. \tag{32}$$

This is identical to the earlier conditions for multiple intersections of the glider track with isopycnals, $\alpha < \Phi_2$ and $\alpha > \Phi_1$, and leads to a value of s below which there are no solutions (e.g., in Figure 8a, when $\theta = 7.13$ deg, $\alpha = 30$ deg, s must exceed 1.276. In Figure 8b, where $\theta = 45$ deg, s must be greater than 5.22 if $\alpha = 40$ deg, exceeding the range of s shown and greater than likely possible oceanic values).

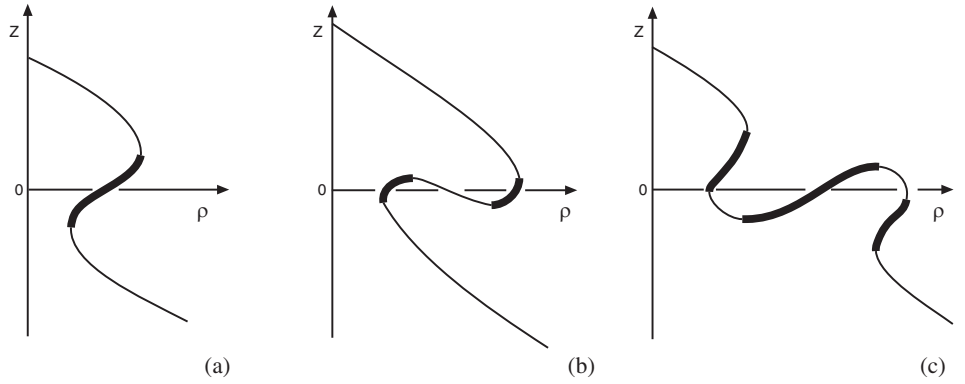

Figure 9. The variation of density measured by the glider as a function of its vertical location, Z. In (a) Z increases monotonically, but in (b) and (c), because of the motion induced by the wave field, the glider is carried downward. The statically unstable regions where the measured density increases with Z are marked by the thickened lines. The relatively small vertical extent of the statically unstable regions in (b) leads to the anomalous curve for ζ at $\alpha = 20$ deg in Figure 8a, as explained in the text.

In general for $V > 0$, relatively small c and $0 < \alpha(\text{deg}) \leq 90$, the glider moves montonically upward, leading to density variations with its vertical position, Z, as illustrated in Figure 9a. If, however, the maximum downward vertical component of the wave induced motion in (26c), $|w| = a\sigma$, exceeds the upward vertical motion of the glider through the water, $V \sin\alpha$, i.e., when $(c/V)s/(\sin\alpha\cos\theta) > 1$, the glider may be carried downward by the wave motion over part of the Doppler shifted period. An example, one that leads to anomalous overturning scales, is found in Figure 8a when $c/V = 0.2$, $\theta = 7.1$ deg and $\alpha = 20$ deg, giving a condition $s > 1.70$ for downward glider motion, although the condition (32) proves less severe, leading to a cut-off at $s = 1.52$. When $1.52 < s < 1.70$, the variation of density at the vertical position, Z, of the glider is as illustrated in Figure 9a, but at greater s the variation is as sketched in Figure 9b. Although the displacement scales, L_T, are relatively large, regions where the measured vertical density gradient, $d\rho/dZ$, is positive are now relatively small as indicated by the thickened lines in Figure 9b, and the overturning scales, Z_0, that must now be calculated over these regions, are therefore small as shown in Figure 8a; the glider-measured overturning scales are not a robust measure of L_T. A further example of downward glider motion is found in Figure 8b when $c/V = 0.2$, $\theta = 45$ deg and $\alpha = 20$ deg, giving $|w| > V\sin\alpha$ if $s > 1.21$. At greater s, the density, ρ, measured by the glider at height, Z, is as shown in Figure 9c, giving relatively large overturning scales, comparable to those in Figure 9a.

Although the overturning scales differ, the displacement scales, L_T, at $\alpha = 90$ deg measured by a free-fall probe displaced from its vertical track by the wave-induced water motion (the dashed curves marked '90' in Fig. 8) are found to be independent of θ and the same as those of Case (a) in Figure 5 ($c/V = 0$). Consequently a free-fall probe ascending or

descending through a field of convectively breaking internal waves will measure the real displacement scales within the overturning waves and L_T will be independent of c/V, at least within the limits assumed here, e.g., that a probe will conform to the wave-induced motions without any time delay and that the statically unstable state of the waves when $s > 1$ is maintained during the passage of the probe.

5. Summary

Proportionality of the displacement scale, L_T, and the Ozmidov length scale, L_{Oz}, is commonly used to obtain estimates of ε, the rate of dissipation of turbulent kinetic energy per unit mass. Eq. (1) implies that the estimated dissipation rate is proportional to the square of the scale of overturns, L_T. As shown in Section 2 and Table 1, the probable errors involved in estimating the overturn scale of K-H billows are greatest when their aspect ratio, b/a, is greatest and when a glider's inclination angle, α, is small, but is unlikely to amount to a factor $2^{-1/2}$ or therefore to an underestimate of ε by a factor as great as 2. Given the commonly wide range of ε values and the usual uncertainty of about 2 in measuring its value using shear foil probes, this underestimate may be relatively insignificant. As shown in Table 2, larger errors are possible, however, in measuring eddies in stratified turbulent flows, and their magnitude depends on the orientation of eddies relative to the trajectory of the glider. The attempts to obtain estimates of probable overturning scales in turbulent eddies draw attention to the paucity of information about the structure of naturally occurring eddies in the stratified ocean.

Attention is also drawn to the false overturns that might be apparent using gliders with small inclination angles, α, in internal waves, an effect that may be augmented when steep waves are superimposed on others. Apparent and spurious breaking may be detected using gliders, and erroneous estimates of the displacement scales obtained, even when the wave slope, s, < 1 and convective overturn is absent (Figs. 7 and 8). Figures 6 and 7 show that the measured overturning scales depend on the azimuthal angle, ϕ; the orientation of a glider path to the internal wave. Except in particular regions (e.g., near continental slopes of in the lee of a ridge) where the wave orientation may be known, the direction of propagation of steep internal waves is presently indeterminate; over relatively short periods of time and moderate distances, the internal wave field may be directionally anisotropic, but more information of wave directionality and its persistence is required. Quantification of overturns from glider measurements of the apparent vertical size of the regions in which the density increases upward can result in misleading estimates of the scale of overturns (exemplified by the case shown in Fig. 9b), and care is consequently required in using gliders to measure displacement scales.

Although, because of the wave-induced horizontal and vertical motions, the trajectory of free-fall probes will not be vertical when passing through an internal wave, and nor will it be steady, the mean square displacements obtained from measurements are found to be the same as those that would be made by a probe passing vertically through a frozen wave

field. Although advected in space by the internal waves, free-fall probes continue to cross isopycnal surfaces at a constant rate, just as if they were frozen. More information is however required of the nature of breaking internal waves in the deep ocean, as well as turbulent eddies, particularly of how to distinguish between shear induced overturns and convective wave breaking, perhaps using fine-scale arrays of high-resolution sensors as suggested by Thorpe (2010).

Acknowledgments. I am grateful for discussions and comments about this paper from Professor W. D. Smyth (the senior author of the companion paper), to Mr. Wei Liu for clarification of Liu *et al.* (2010), to Mrs. Kate Davis for assistance in preparing the figures, and to Professor Alan Davies for use of a computer.

APPENDIX

Braids, at angles α_1 to the horizontal, are roughly tangential to billows. A braid shown in Figure 1b, passes through the point $(\lambda/2, 0)$, where λ is the billow wavelength. Using (6) and equating the braid slope to $\tan^{-1}(b/a)$, we find $\lambda = (2\sqrt{2})a$. As can also be inferred from Figure 1b, a glider path can intersect a third billow if $\alpha < \alpha_2$ where the tangent at angle α_2 passes through the point $(\lambda, 0)$, (6) then giving $\lambda^2 = a^2 + b^2 \cot^2 \alpha_2$, or with $\lambda = (2\sqrt{2})a$, $\alpha_2 = \tan^{-1}[b/(\sqrt{7}a)]$. The largest value of b/a is 0.5, and so $\alpha_2 \leq 10.7$ deg., smaller than the typical glider paths. Generally, at most, a glider will intersect only two billows.

Figure 1c shows a glider path, AB, at inclination $\alpha_2 < \alpha < \alpha_1$ that intersects two billows and passes through the point $X = (x, 0)$, where $OX = x$. Extending (6), the vertical distance, $z_B - z_A$, between the points A and B is found to be given by,

$$z_B - z_A = (b/y^2)\{b\lambda \cot \alpha + a[(y^2 - x^2)^{1/2} + (y^2 - (\lambda + x)^2)^{1/2}]\},$$

where $y = aq = [a^2 + b^2 \cot^2 \alpha]^{1/2}$. The points $X_3 = \lambda - y$ and $X_4 = y$ give the range of the point X, corresponding to a glider path passing through two billows: the mean square of $(z_B - z_A)$ of such a path can be found numerically for given α and b/a. The mean square billow height where the glider path only crosses a single billow (e.g., the line CD, for values of x between O to X_3 in Fig. 1c) is found by integrating $(z_1 - z_2)^2$ given by (5) and doubling the resultant value to cover the range of $x < 0$. Summing the mean square values, weighted by the ranges O to X_3 and X_3 to X_4 and taking the square root, gives the rms height that would be observed by the glider at inclination α. Division by the rms height observed by a vertically moving probe over one billow but averaged over a length OX_4 then leads to a revised value of *Bf*.

REFERENCES

Dillon, T. M. 1982. Vertical overturns: a comparison of Thorpe and Ozmidov length scales. J. Geophys. Res., *87*, 9601–9613.

Eriksen, C. C. 2009. 'Gliders,' Encyclopedia of Ocean Sciences, 2nd ed., J. H. Steele, S. A. Thorpe and K. K.Turekian, eds., Elsevier/Academic Press, Boston, *3*, 59–66.

Ferron, B., H. Mercier, K. Speer, A. Gargett, and K. Polzin. 1998. Mixing in the Romanche Fracture Zone. J. Phys. Oceanogr., *28*, 1929–1945.

Keller, K. H. and C. W. Van Atta. 2000. An experimental investigation of the vertical temperature structure of homogeneous stratified shear turbulence. J. Fluid Mech., *425*, 1–29.

Lawrence, G. A., F. K. Browand and L. G. Redekopf. 1991. The stability of a sheared density interface. Phys. Fluids A, *3*, 2360–2370.

Lazier, J. R. N. and H. Sandstrom. 1978. Migrating thermal structure in a freshwater thermocline. J. Phys. Oceanogr., *8*, 1070–1079.

Linden, P. F. 1975. The deepening of a mixed layer in a stratified fluid. J. Fluid Mech., *71*, 385–405.

Liu, W., F. Bretherton, Z. Liu *et al*. 2010. Breaking of progressive internal waves: convective instability and shear instability. J. Phys. Oceanogr., *40*, 2243–2263.

Marmorino, G. O. 1987. Observations of small-scale mixing processes in the seasonal thermocline. Part II: wave breaking. J. Phys. Oceanogr., *17*, 1348–1355.

Osborn, T. R. 1980. Estimates of the local rate of vertical diffusion from dissipation measurements. J. Phys. Oceanogr., *10*, 83–89.

Ozen, B., S. A. Thorpe, U. Lemmin and T. R. Osborn. 2006. Cold-water events and dissipation in the mixed layer of a lake. J. Phys. Oceanogr., *36*, 1928–1939.

Ozmidov, R. V. 1965. On the turbulent exchange in a stably stratified ocean. Izvestia, Acad. Sci. U.S.S.R., Atmos. & Ocean Phys., *1*, 861–871.

Pawlak, G. and L. Armi. 1998. Vortex dynamics in a spatially accelerating shear layer. J. Fluid Mech., *376*, 1–35.

Peters, H., M. C. Gregg and J. M. Toole. 1988. On the parameterization of equatorial turbulence. J. Geophys. Res., *93*, 1199–1218.

Smyth, W. D. and S. A. Thorpe. 2012. Glider measurements of overturning in a Kelvin- Helmholtz billow train. J. Mar. Res., *70*, 119–140.

Strang, E. J. and H. J. S. Fernando. 2001. Entrainment and mixing in stratified shear flows. J. Fluid Mech., *428*, 349–386.

Sutherland, B. R. and P. F. Linden. 1998. Internal wave excitation from a stratified flow over a thin barrier. J. Fluid Mech., *377*, 223–252.

Thorpe, S. A. 1968. A method of producing a shear flow in a stratified fluid. J. Fluid Mech., *32*, 693–704.

—— 1971. Experiments on the instability of stratified shear flows: miscible fluids. J. Fluid Mech., *46*, 299–319.

—— 1973. Experiments on instability and turbulence in a stratified shear flow. J. Fluid Mech., *61*, 731–751.

—— 1977. Turbulence and mixing in a Scottish loch. Phil. Trans. Roy. Soc. Lond. A, *286*, 125–181.

—— 1978. The near-surface ocean mixing layer in stable heating conditions. J. Geophys. Res., *83*, 2875–2885.

—— 1994. Statically unstable layers produced by overturning internal gravity waves. J. Fluid Mech., *260*, 333–350.

—— 2002. The axial coherence of Kelvin-Helmholtz billows. Quart. J. Roy. Meteorol. Soc., *128*, 1529–1542.

—— 2010. Breaking internal waves and turbulent dissipation. J. Mar. Res., *68*, 851–880.

Thorpe, S. A. and A. J. Hall. 1977. Mixing in upper layer of lake during heating cycle. Nature, *265*, 719–722.

Thorpe, S. A. and A. J. Hall, C. Taylor and J. Allen. 1977. Billows in Loch Ness. Deep-Sea Res., *24*, 371–379.

Van Haren, H. and L. Gostiaux. 2010. A deep-ocean Kelvin-Helmholtz billow train. Geophys. Res. Letts., *37*, L03605, doi:10.1029/2009GL041890.

Wesson, J. C. and M. C. Gregg. 1994. Mixing at the Camarinal Sill in the Strait of Gibraltar. J. Geophys. Res., *99*, 9847–9878.

Woods, J. D. 1968. Wave-induced shear instability in the summer thermocline. J. Fluid Mech., *32*, 791–800.

Received: *31 May, 2011*; revised: *29 November, 2011*.